References and Notes

(1) (a) W. Kirmse, "Carbene Chemistry", 2nd ed., Academic Press, New York, 1971; (b) M. Jones and R. A. Moss, "Carbenes", Vol. 1, Wiley, New York, 1973; (c) D. Bethell in "Organic Reactive Intermediates", S. P. McManus, Ed., Academic Press, New York, 1973, Chapter 2; (d) J. Hine, "Divalent Carbon", Ronald Press, New York, 1964.
(2) D. E. Milligan and M. E. Jacox, *J. Chem. Phys.*, **47**, 703 (1967).
(3) L. Andrews, *J. Chem. Phys.*, **48**, 979 (1968).
(4) A. K. Maltsev, R. H. Hauge, and J. L. Margrave, *J. Phys. Chem.*, **75**, 3984 (1971).
(5) D. A. Hatzenbuhler, L. Andrews, and F. A. Carey, *J. Am. Chem. Soc.*, **97**, 187 (1975).
(6) L. Andrews, J. M. Grzybowski, and R. O. Allen, *J. Phys. Chem.*, **79**, 904 (1975).
(7) F. T. Prochaska and L. Andrews, *J. Chem. Phys.*, **67**, 1091 (1977).
(8) F. T. Prochaska and L. Andrews, *J. Am. Chem. Soc.*, **100**, 2102 (1978).
(9) C. A. Wight, B. S. Ault, and L. Andrews, *J. Chem. Phys.*, **65**, 1244 (1976).
(10) L. Andrews, H. Willner, and F. T. Prochaska, *J. Fluorine Chem.*, **13**, 273 (1979).
(11) L. Andrews, F. T. Prochaska, and B. S. Ault, *J. Am. Chem. Soc.*, **101**, 9, (1979).
(12) L. Andrews, C. A. Wight, F. T. Prochaska, S. A. McDonald, and B. S. Ault, *J. Mol. Spectrosc.*, **73**, 120 (1978).
(13) M. E. Jacox and D. E. Milligan, *Chem. Phys.*, **16**, 195 (1976).
(14) B. W. Keelan and L. Andrews, to be published.
(15) F. T. Prochaska, B. W. Keelan, and L. Andrews, *J. Mol. Spectrosc.*, to be published.
(16) C. E. Smith, D. E. Milligan, and M. E. Jacox, *J. Chem. Phys.*, **54**, 2780 (1971).
(17) D. E. Milligan, M. E. Jacox, J. H. McAuley, and C. E. Smith, *J. Mol. Spectrosc.*, **45**, 377 (1973).
(18) T. G. Carver and L. Andrews, *J. Chem. Phys.*, **50**, 4235 (1969).
(19) F. T. Prochaska and L. Andrews, *J. Chem. Phys.*, **68**, 5568 (1978).
(20) H. M. Rosenstock, K. Draxl, B. W. Steiner, and J. T. Herron, *J. Phys. Chem. Ref. Data*, **6**, No. 1 (1977).
(21) F. T. Prochaska and L. Andrews, *J. Chem. Phys.*, **68**, 5577 (1978).
(22) D. E. Milligan and M. E. Jacox, *J. Chem. Phys.*, **48**, 2265 (1968).
(23) L. Andrews and F. T. Prochaska, *J. Phys. Chem.*, **83**, 824 (1979).
(24) J. M. Dyke, L. Golob, N. Jonathan, A. Morris, and M. Okuda, *J. Chem. Soc., Faraday Trans. 2*, **70**, 1828 (1974).
(25) J. S. Shapiro and F. P. Lossing, *J. Phys. Chem.*, **72**, 1552 (1968).
(26) J. Vogt and J. L. Beauchamp, *J. Am. Chem. Soc.*, **97**, 6682 (1975).
(27) B. A. Levi, R. W. Taft, and W. J. Hehre, *J. Am. Chem. Soc.*, **99**, 8454 (1977).
(28) J. P. Lowe, unpublished calculation (1979).

Selective Naked-Cluster Cryophotochemistry and SCF-Xα-SW Calculations for Cu_2 and Ag_2

Geoffrey A. Ozin,* Helmut Huber, Douglas McIntosh, Steven Mitchell, Joe G. Norman, Jr.,*† and Louis Noodleman

Contribution from the Lash Miller Chemical Laboratory and Erindale College, University of Toronto, Toronto, Ontario, Canada, and the Department of Chemistry, University of Washington, Seattle, Washington 98195.

Received September 11, 1978

Abstract: The concept of conducting photoselective transformations on small, well-defined, ligand-free transition metal clusters is explored for the first time by investigating the visible (370–390 nm) photochemistry of Ar- and Kr-entrapped Cu_2 and Ag_2. With prior knowledge of the 200–900-nm optical spectra of Cu_{1-3} and Ag_{1-4} clusters, generated either by metal atom deposition or photoclustering techniques, one can rationalize the observed Cu_2 and Ag_2 visible cryophotochemistry in terms of a highly selective matrix-induced photodissociation step for which a mechanism involving formation of a metal atom–matrix atom(s) exciplex is proposed. SCF-Xα-SW MO calculations for Cu_2 and Ag_2 confirm that the wavelengths used for the photoexcitations are essentially those of the electronic transitions from the main bonding to the main antibonding orbital (i.e., $s\sigma_g \rightarrow s\sigma_u$), thus providing a description of the excited states which is useful in accounting for the observed photochemistry. The calculations represent the most thorough theoretical study of Cu_2 and Ag_2 to date. Complete potential curves are calculated and the observed r_e, D_e, and ν(M–M) are in good agreement with experiment. The bonding at the likely equilibrium distances is discussed; that in Ag_2 is found to be almost purely s, while in Cu_2 there appears to be a minor d contribution. The electronic spectra are assigned in detail from transition-state calculations of both energies and oscillator strengths. The A←X, C←X, and E←X systems of Ag_2 are attributed to $s\sigma \rightarrow s\sigma^*$, $s\sigma \rightarrow p\pi$, and $d\pi^* \rightarrow s\sigma^*$ transitions, respectively. The A←X and B←X systems of Cu_2 are ascribed to $d\pi^* \rightarrow s\sigma^*$ and $s\sigma \rightarrow s\sigma^*$ excitations, and the UV bands of Cu_2 near 260, 235, and 220 nm are assigned to mainly $d\pi^* \rightarrow p\pi$, $s\sigma \rightarrow p\pi$, and $d\sigma \rightarrow s\sigma^*$ processes, respectively.

Introduction

Recent work in our laboratory has demonstrated that small metallic[1] and bimetallic[2] clusters of known composition can be efficiently generated in low-temperature, weakly interacting matrix supports by narrow-band photoexcitation of the resonance lines of matrix-entrapped metal atomic species. The highly controlled nature and photoselectivity of the aggregation processes involved have recently been unveiled in a series of M/M′/Ar(Kr) bimetallic experiments[2,3] (where M = Cr; M′ = Mo or Ag) in which the following sequence of nucleation events was observed:

$$\left.\begin{array}{l} M^\dagger + M^\dagger \rightarrow M_2 \\ M^\dagger + M_2 \rightarrow M_3 \\ M^\dagger + MM' \rightarrow M_2M' \\ M^\dagger + M' \rightarrow MM' \\ M^\dagger + M'_2 \rightarrow MM'_2 \end{array}\right\} \text{M photomobilization (no } M'_2, M'_3 \text{ clusters observed)}$$

† Fellow of the Alfred P. Sloan Foundation, 1978–1980.

$$\left.\begin{array}{l} M'^\dagger + M'^\dagger \rightarrow M'_2 \\ M'^\dagger + M'_2 \rightarrow M'_3 \\ M'^\dagger + MM' \rightarrow MM'_2 \\ M'^\dagger + M \rightarrow MM' \\ M'^\dagger + M_2 \rightarrow M_2M' \end{array}\right\} \text{M′ photomobilization (no } M_2, M_3 \text{ clusters observed)}$$

(where $M^\dagger$ and $M'^\dagger$ represent photomobilized M and M′, respectively).

Recent emission experiments by Kolb and co-workers[4a] and Ozin, Kenney-Wallace, and co-workers,[4c] employing 300–330-nm excitation of Ag atoms in inert gas matrices, have revealed the presence of several intense emission bands. In the cases of argon and krypton the largest Stokes shift corresponds to the most intense band which is centered in the region 400–500 nm. The large Stokes shift suggests the existence of a significant nonradiative energy channel following Ag atom photoexcitation, of which the observed metal atom photomobility is presumably a manifestation. At the present time we

0002-7863/79/1501-3504$01.00/0

would suggest the following simplified scheme which seems most consistent with our available experimental information. This scheme represents a qualitative model within the context of which we can explain both the photomobilization and emission which occurs following 300-nm excitation of matrix-entrapped Ag atoms. However, future studies[4c] on the time dependence and polarization properties of the emissions may well reveal a more complex mechanism. We will refer to this scheme later in our discussion of Cu_2 and Ag_2 cryophotochemistry. The scheme involves (1) ground-state $^2S_{1/2}$ Ag atom photoexcitation to the $^2P_{1/2,1/2}$, $^2P_{3/2,3/2}$, $^2P_{3/2,1/2}$ excited states;[4b] (2) exciplex formation involving at least two exciplex electronic states and involving one or more rare-gas atoms for each excited Ag atom, possibly followed by vibrational relaxation of the excited exciplex states (a minimum of two excited exciplex states is strongly suggested by the emission spectra[4a-c]); (3) exciplex fluorescence, again involving at least two excited exciplex electronic states, to the ground (repulsive) state; (4) dissociation of the repulsive ground exciplex state resulting in Ag atom mobilization.

We note with reference to point (2) that exciplex formation between matrix-entrapped metal atoms and rare gas matrix atoms has been suggested by a number of workers to explain certain effects observed in the absorption and luminescence spectra of matrix-isolated metal atoms.[4a,c,d,7b]

The inherent photoselectivity of these metal-atom clustering processes immediately suggests the possibility of conducting "selective, naked cluster cryophotochemistry" using narrow-band photoexcitation of various molecular absorptions of M_n species.[5] As a first attempt to evaluate this proposal in detail we have performed a series of Cu_2 and Ag_2 photochemical experiments involving irradiation near 400 nm, where the lowest energy absorptions of Cu_2 and Ag_2 occur.

Cu_2 and Ag_2 are particularly appropriate to such experiments for two reasons. Firstly, their spectra have been rather thoroughly studied, both in the gas phase at high temperatures[6] and in inert-gas matrices at low temperatures.[7] Vibration-rotation analyses of the gas-phase spectra have produced precise values for the $0 \rightarrow 0$ transition energies, metal-metal stretching frequencies, and, for Cu_2, the internuclear distance (2.2195 Å). Dissociation energies have been obtained from mass spectra.[8] The assignments proposed for the observed electronic transitions from the experiments and from simple MO calculations of the extended Hückel or CNDO type[9] serve as a guide to selection of transitions for the photochemical studies.

Secondly, the inherently simple electronic structures expected for Cu_2 and Ag_2 further aid the design and interpretation of the photochemical experiments. The metal-metal bonds should largely involve simple pairing of the s electrons on the two $d^{10}s^1$ metal atoms. One of the lowest energy absorptions should therefore involve excitation from the bonding $s\sigma_g$ to the antibonding $s\sigma_u$ orbital.

The gas-phase spectra strongly suggest that the apparent $s\sigma_g \rightarrow s\sigma_u$ excited states of Cu_2 and Ag_2 are bound, with extensive vibrational structure being observed.[6] However, the results of the present study indicate that the behavior of these excited states in a condensed matrix phase is quite different from that which is observed in gas-phase studies. As will be seen below, our interpretation of irradiation near 400 nm in this context suggests that the factors which are important in the above scheme are also important in determining the fate of the excited molecular states of matrix-entrapped Cu_2 and Ag_2.

We also report SCF-Xα-SW calculations on Cu_2 and Ag_2. These provide an interpretation of the electronic spectra which is consistent with the observed photochemistry. In their own right, they represent the most thorough and, we believe, a quite accurate theoretical treatment of the spectra, orbital structure, and potential curves of Cu_2 and Ag_2. Previously in this area we reported Xα-SW calculations for Cr_2, CrMo, and Mo_2,[10a] and preliminary results for Rh_2.[10b]

Experimental Section

Photochemistry. Monatomic Cu and Ag vapor was generated by directly heating a tantalum filament around the center of which was wound 0.010-in. diameter Cu or Ag wire, respectively. The evaporation furnace was identical with that described previously.[11] The Cu (99.999%) was supplied by McKay, New York, and the Ag (99.999%) by Imperial Smelting Company, Toronto. The rate of Cu and Ag atom deposition was continuously monitored using a quartz crystal microbalance built into the furnace-cryostat assembly.[12]

In the optical experiments matrices were deposited onto a NaCl optical window cooled to 12 K by means of an Air Products Displex closed-cycle helium refrigerator. UV-visible spectra were recorded on a Varian Techtron or Unicam 8000 spectrophotometer in the range 200–900 nm.

Photolyses were performed with an Oriel 450-W xenon lamp and Schoeffel monochromator assembly using a 20-nm band-pass in the 300–400-nm region.

SCF Calculations. Converged results were obtained for Cu_2 at 17 bond distances in the range 1.95–2.52 Å, and for Ag_2 at 16 distances in the range 2.23–2.95 Å. Schwarz' α_{HF} exchange parameters[13] of 0.706 97 for Cu and 0.710 45 for Ag were used. Overlapping-sphere atomic radii at each distance were taken as 85% of the values enclosing the atomic number of electrons in the initial superimposed-atom charge density.[14] Touching outer-sphere radii were used. Spherical harmonics through $l = 2$ and 4 were used to expand the wave functions in the atomic and outer regions, respectively. Core energy levels were never frozen; in each iteration they were calculated explicitly using only the surrounding-atomic-sphere potential. The 3s and 3p levels of Cu, and the 4s and 4p levels of Ag, were treated as valence levels to increase the accuracy of the potential curves.

Potential Curves. The equilibrium bond distance, force constant, and minimum total energy for each molecule were obtained by a quadratic fit to the total energy vs. distance values. The dissociation energy was calculated as the difference between the minimum total energy and twice the hyper-Hartree–Fock atomic energies of Mann;[15] this is the proper procedure when the α_{HF} exchange parameters are used in the molecular calculations.[13]

Excited States. The SCF ground-state potentials for Cu_2 at 2.22 Å and for Ag_2 at 2.84 and 2.47 Å were used to begin transition-state calculations of the electronic spectra. Two different spin-unrestricted calculations were done for all dipole-allowed transitions below 52 000 cm^{-1}, to give predictions of the triplet and average of the singlet and triplet energies, respectively. Combination of the two numbers allows explicit prediction of the singlet (spin-allowed) energy.[16] Cu and outer sphere radii were 2.704 and 4.802 bohr, respectively. Ag and outer sphere radii were 3.247 and 5.931 bohr at 2.84 Å and 2.859 and 5.913 bohr at 2.47 Å, respectively. Here 1 bohr = 0.529 177 Å.

Oscillator strengths f were calculated for each transition using the orbitals and potential from the singlet-triplet average transition state, according to the procedure of Noodleman.[16a] Two sets of f's were obtained, the first with the same spherical harmonics as for the SCF calculations, the second with the atomic basis set expanded to $l_{max} = 4$. Inspection of individual matrix elements showed angular-momentum convergence of f values within a few percent at the level of the larger basis set, for which we report results here.

Results and Discussion of Photochemistry

A typical series of optical spectral traces which illustrate the cryophotochemistry of Ag_2 is shown in Figure 1. For instance, Figure 1A shows the absorptions of isolated Ag atoms in the presence of small amounts of Ag_2 molecules, obtained after a Ag/Ar $\simeq 1/10^4$ deposition at 12 K. Under these concentration conditions the outcome of 315-nm narrow-band photoexcitation (20 nm bandwidth, from an Oriel 450-W xenon lamp–Schoeffel monochromator system) of the $^2S_{1/2} \rightarrow {}^2P_{3/2,1/2}$ resonance lines of atomic silver is photoaggregation up to the Ag_3 stage (identical with that reported earlier[1,17]) as depicted in Figure 1B. The decay of Ag and growth of Ag_2 and Ag_3 are also represented in graphical form in Figure 2. A

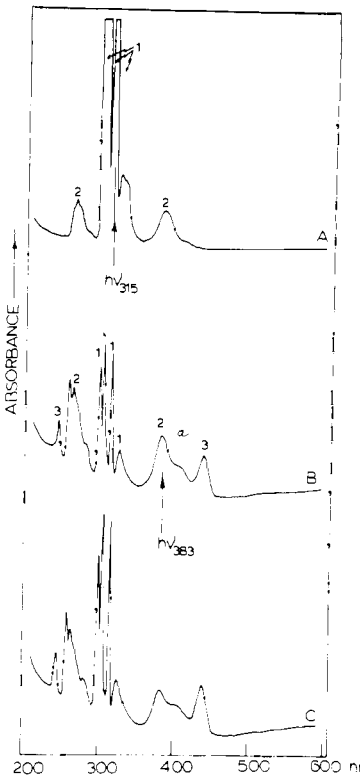

Figure 1. The optical spectrum of Ag/Ar ≃ $1/10^4$ deposited at 12 K: (A) showing isolated Ag atoms and Ag_2 molecules; (B) after 40 min 315-nm narrow-band continuous photoexcitation of the Ag atomic resonance lines, showing photoaggregation to the $Ag_{2,3}$ stage; (C) after 15 min 383-nm narrow-band continuous photoexcitation of the lowest energy transition of Ag_2, showing photodissociation to Ag atoms and subsequent aggregation. The Ag_2 low-energy shoulder labeled (a) is thought to be a site-splitting effect (see text).

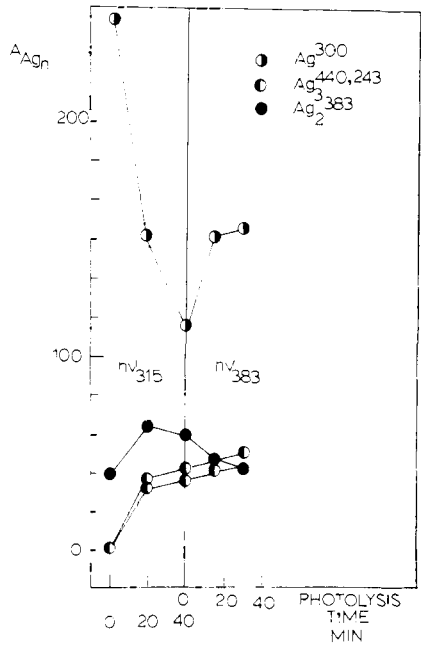

Figure 2. Graphical representation of the optical absorbance changes for $Ag_{1,2,3}$ as a function of photolysis time for both Ag^{315} and Ag^{383} excitation.

similar set of observations has been made for Cu_2 and is illustrated in Figures 3 and 4.

With the distribution of $Ag_{1,2,3}$ clusters shown in Figure 1B, one can turn to 383-nm narrow-band excitation and thereby

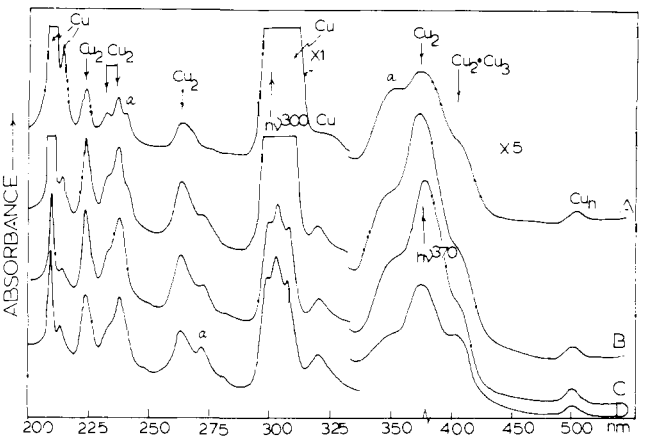

Figure 3. The optical spectrum of Cu/Ar ≃ $1/10^4$ at 12 K: (A) showing isolated Cu atoms and Cu_2 molecules; (B–C) photoaggregation as the result of two 30-min irradiations of the resonance lines of Cu atoms at 302 nm; (D) photodissociation of Cu_2 resulting from a 30-min irradiation at the 370-nm band of Cu_2. The features marked (a) are thought to arise from secondary trapping sites of Cu_2 (see text). Note scale change between 325 and 400 nm.

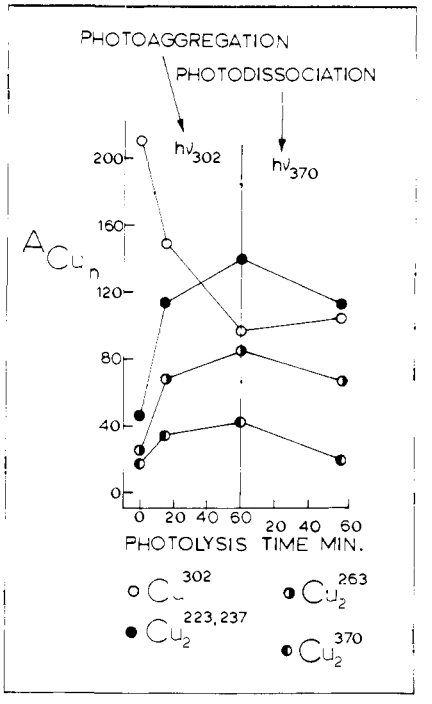

Figure 4. Graphical representation of the optical absorbance changes shown in Figure 3. The points representing Cu_2 bands are shown on a fivefold expanded scale for both Cu^{302} and Cu_2^{370} excitation.

test the feasibility of selective photodissociation and nucleation events associated with disilver itself. For example, the outcome of 15 min continuous irradiation of Ag_2 is illustrated in Figures 1C and 2. Immediately apparent from these optical spectra is the dramatic growth of the Ag atomic resonance lines. Noticeable, however, is the concomitant *growth* of Ag_3 yet *decay* of Ag_2 under these matrix concentration conditions.

A similar series of optical spectra illustrating photoaggregation of Ag atoms and photodissociation of Ag_2 in a Kr matrix is shown in Figure 5, where 390-nm excitation of Ag_2 is seen to result in a substantial decrease in the Ag_2 bands and a relatively small but significant increase in the atomic resonance lines. The shoulder near 280 nm (marked (a) in Figure 5C) is believed to be due to an unstable trapping site of Ag_2 in solid Kr. Ag_2 molecules in this site apparently resist photodisso-

ciation but exhibit thermal instability as demonstrated by the near disappearance of this shoulder on annealing the matrix near 30 K. (An entirely analogous effect has been observed for Cu_2 in Ar matrices, Figure 3D.) Notable in the case of the Kr matrices (Figure 5) is the spectroscopic absence of Ag_3. However, in the case of higher concentrations of Ag in a Kr matrix the presence of Ag_3 following photoaggregation does become evident in the optical spectrum. Under these conditions Ag_2 visible photoexcitation results in (a) Ag_2 decay, (b) essentially zero growth of Ag, (c) Ag_3 decay, and (d) slight Ag_4 growth.

It is clear from the observations described above that the end result of Ag_2 visible photoexcitation, in terms of the observed yield of isolated atoms as the photodissociation products, is strongly dependent upon the concentration conditions employed, but that the excitation invariably results in a reduction of the Ag_2 concentration. A similar observation applies for the Cu_2 photoexcitations. In the case of both Cu_2 and Ag_2 the observed yield of isolated atoms generally increases with decreasing total metal concentration. Typical yields are low, being near 20% for both Cu_2/Ar (Figure 3) and Ag_2/Kr (Figure 5). The percentage yield of isolated atoms has been found to depend on other factors as well, such as the extent of photoaggregation preceding Cu_2 or Ag_2 photoexcitation and the Ag_2/Cu_2 (390/370 nm) excitation conditions (intensity and irradiation time), but no systematic study of these variables has as yet been undertaken.

It will be useful in the following discussion of our results to refer to some recent emission studies[4c] which relate to emission bands observed following 260- or 390-nm excitation of Ag_2 in Ar matrices. For the purposes of the present discussion the most important result of these emission measurements is that, regardless of which Ag_2 excitation is used, part of the observed emission[28] corresponds with certain emission bands observed for $^2S_{1/2} \rightarrow {}^2P_{1/2,3/2}$ Ag excitations, implying that the emitting species is the same for both Ag and Ag_2 photoexcitations. According to the preceding scheme the emission is due to transitions between certain excited states and the ground state of a Ag atom-noble gas exciplex. Thus, we are lead to the conclusion that the $s\sigma_g \rightarrow s\sigma_u$ ($^1\Sigma_g^+ \rightarrow {}^1\Sigma_u^+$) excitation of Ag_2, to which the 390-nm band is assigned in the following section, ultimately results in the formation of the above-mentioned exciplex excited states. It is proposed in the scheme that radiative decay of these excited states is followed by dissociation to form a mobile ground-state Ag atom.

The important step of our proposed mechanism for Ag_2 photodissociation involves Ag–Ag bond breaking in the excited $^1\Sigma_u^+$ state [O_u^+ in the case of (J–J) coupling], and simultaneous Ag–Ar bond formation to form an excited-state complex. This step amounts to a transfer of electronic excitation from Ag_2 to $Ag(Ar)_n$ and elimination of a ground-state Ag atom. The final step of the photodissociation, following radiative decay of the excited exciplex states, would then be dissociation of the repulsive ground exciplex state, thus producing a second (mobile) ground-state Ag atom.

Although we have not yet undertaken quantum efficiency measurements, the emission bands resulting from 390-nm Ag_2 excitation appear quite intense. The formation of mobile ground-state Ag atoms as a result of Ag_2 visible photoexcitation may explain the low yield of isolated atoms, since the mobile photodissociation products are potentially reactive in subsequent aggregation processes. Finally, we note that the $^1\Sigma_u^+$ state of Ag_2 correlates best with a $^2S + {}^2P$ separated atom limit,[6b] and that ^2P atoms are produced as a result of the atomic excitations. Hence, it is not unreasonable to suggest that the emitting species is the same for both 390-nm Ag_2 and 300-nm Ag excitations.[28]

In future studies we plan to critically examine the proposals outlined in the scheme. These studies will include (1) quantitative measurements involving lifetimes of the excited states, polarizations of and quantum efficiencies for fluorescence; (2) SCF-Xα-SW molecular orbital calculations of models for the optical properties of the proposed exciplex;[29] (3) correlation of the emission data for various matrix supports with the kinetic characteristics[4c,17] of the photoaggregation processes in the respective matrices.

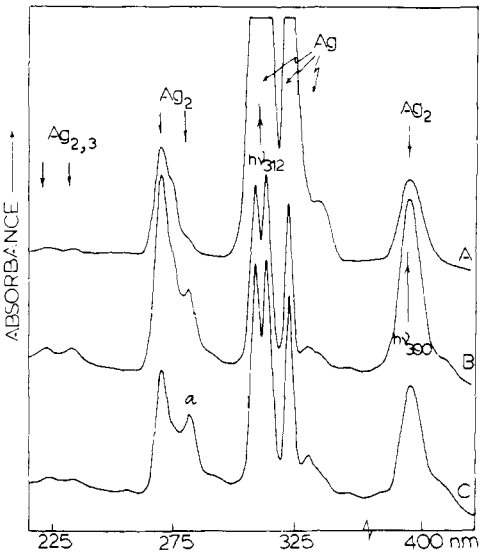

Figure 5. The optical spectrum of Ag/Kr ≃ $1/10^4$ deposited at 12 K: (A) showing isolated Ag atoms and Ag_2 molecules; (B) after 30 min 312-nm narrow band continuous photoexcitation of the Ag atomic resonance lines, showing photoaggregation to the Ag_2 stage; (C) after 70 min 390-nm excitation of Ag_2, showing mainly Ag_2 photodissociation to Ag atoms. The Ag_2 high-energy band labeled (a) is thought to be a site-splitting effect (see text). Note scale change between 325 and 400 nm.

SCF-Xα-SW Calculations

Potential Curves. The overlapping-sphere version of the Xα-SW method has proven generally successful for calculating properties related to the one-electron orbitals of molecules; these include photoelectron, electronic, and ESR spectra, certain features of structure and reactivity, and recently deformation densities.[18,21] However, very few calculations of molecular potential energy surfaces have appeared, primarily because the total energies calculated by the present version of the method should not even in principle reflect the full accuracy of the one-electron orbitals. The reason is that the total electronic charge density obtained by superposition of these orbitals is spherically averaged within each atomic sphere, and volume averaged in the intersphere region, before the total energy is calculated. Although no calculations have appeared, one can imagine the disastrous effect this approximation would have on the calculated bond angles in a molecule containing lone pairs. The limited data available suggests that bond lengths are not as seriously affected; e.g., the discrepancy with experiment for CO, N_2, F_2, and UF_6 averages 0.10 Å.[22,23] However, this is not sufficient accuracy for many chemical purposes, and we have no confidence that the present approximate total energy has any general predictive value.

Efficient use of the real Xα-SW total density to calculate the total energy remains an unsolved problem, although notable progress has been made.[24] The one case where we feel the present approximate total energy should yield a reasonable potential curve is where the bonding is mainly due to interaction of s orbitals—i.e., spherically symmetric densities around each atom. The comparison of our calculated potential curves for Cu_2 and Ag_2 with experiment, shown in Table I, supports this hypothesis.

The metal–metal stretching frequencies, reflecting the shape

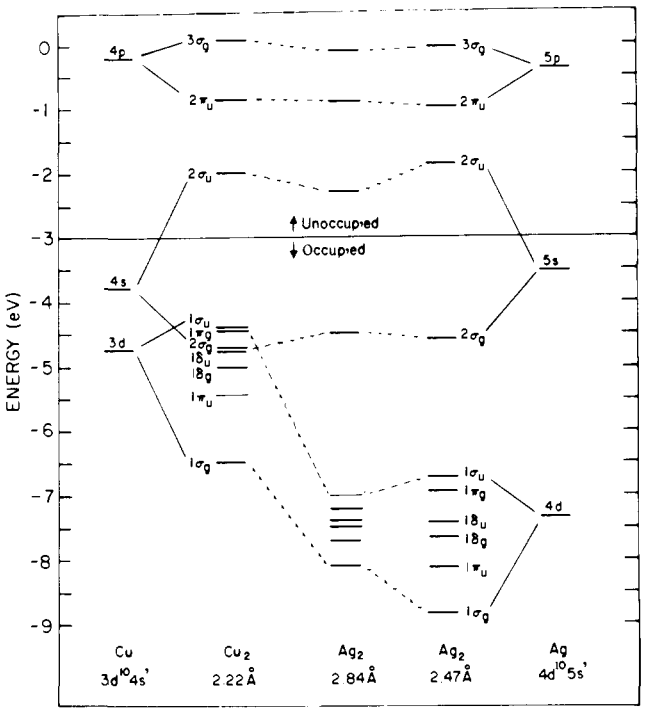

Figure 6. Ground-state SCF-Xα-SW valence energy levels for Cu, Cu_2, Ag_2, and Ag. The bands of molecular levels most closely correlating with atomic d, s, and p levels are indicated.

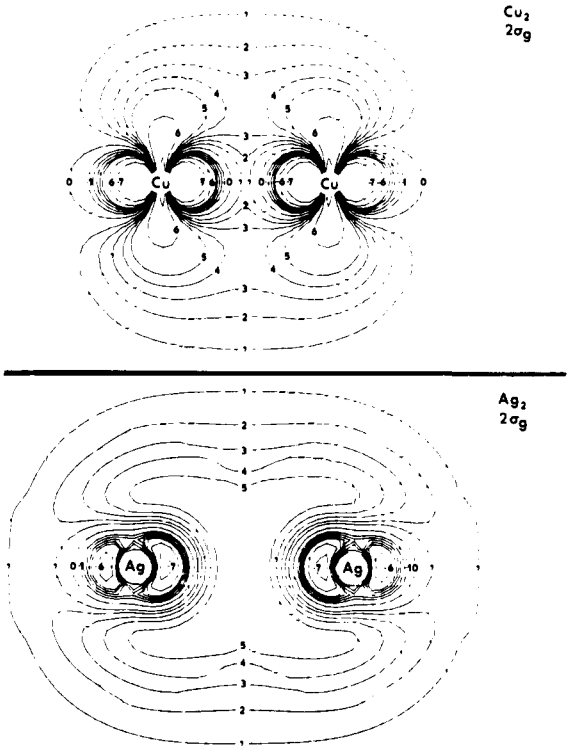

Figure 7. Contour maps of the wave functions for the mainly s bonding orbitals of Cu_2 and Ag_2 at 2.22 and 2.84 Å, respectively. The map of Ag_2 at 2.47 Å is similar. Note the significant amount of d character in the Cu_2 case. The contour values for these maps and Figure 8 are 0, 1, 2, 3, 4, 5, 6, 7 = 0, 0.02, 0.03, 0.04, 0.05, 0.06, 0.09, 0.15, respectively.

Table I. Equilibrium Bond Distances, Metal-Metal Stretching Frequencies, and Dissociation Energies for Cu_2 and Ag_2[a]

	r_e, Å	ν(M-M), cm^{-1}	D_e, kcal/mol
		Cu_2	
calcd	2.17	272 ± 5	66 ± 1
exptl	2.22[b]	266[c]	45 ± 2[d]
		Ag_2	
calcd	2.84	187 ± 2	36 ± 3
exptl	?	192[c]	38 ± 2[d]

[a] Where estimated errors are not indicated, they are smaller than the last figure tabulated. [b] Reference 6d. [c] Reference 6e. [d] Reference 8.

of the curves, are calculated within 6 cm^{-1} of experiment. The bond distance for Cu_2 is within 0.05 Å of experiment. The dissociation energy for Ag_2 is in exact agreement with the measured value; while that for Cu_2 is slightly high, this quantity is well-known to be especially difficult to calculate from first principles by even the best SCF total energy methods.

No experimental bond distance is available for Ag_2. We consider it likely, however, that our predicted value is even more accurate than for Cu_2. The reason is that we calculate the bonding in Ag_2 at all distances to be almost purely s in character, whereas we find a minor d contribution for Cu_2 (see below). The approximate total energy should thus be better for the former; a possible indication of this is the more accurate calculated dissociation energy for Ag_2 than Cu_2.

Against our claim of an accurate predicted Ag-Ag distance should be cited the apparently reliable determination of Au-Au = 2.47 Å in Au_2.[25] However, the measured dissociation energies of Cu_2, Ag_2, and Au_2 are 45, 38, and 53 kcal/mol, respectively;[8] coupled with the measured distances in Cu_2 and Au_2, it thus seems likely that the actual distance in Ag_2 is considerably longer than the 2.47 Å estimated by others.[6f] To cover all possibilities, however, we report below one-electron properties for Ag_2 at both 2.84 and 2.47 Å, using both, along with those for Cu_2 at the experimental distance of 2.22 Å, to discuss the equilibrium one-electron properties of the two molecules.

Ground-State Bonding. Table II summarizes the one-electron energies and orbital compositions for Cu_2 at 2.22 Å and for Ag_2 at 2.84 and 2.47 Å. The energies are compared with those for Cu and Ag atoms in Figure 6. The bound valence orbitals include, in order of increasing energy, the six completely filled σ, π, and δ bonding and antibonding d-band levels, the s band with an occupied σ bonding and empty σ antibonding level, and empty π and σ bonding levels from the p band.

The major difference between the two molecules is that the s band overlaps the upper part of the d band in Cu_2, while the two are very well separated in Ag_2. The d-like $1\sigma_u$ and $1\pi_g$ levels are thus the highest occupied in Cu_2, rather than the $2\sigma_g$ level as in Ag_2. As can be seen from Figure 6, this is a consequence of the much smaller separation of the d and s atomic levels in Cu than in Ag. It leads in Cu_2 to some mixing of 4s character into the formally 3d-derived $1\sigma_g$ orbital, and 3d character into the formally 4s-derived $2\sigma_g$ orbital. In contrast, the $1\sigma_g$ orbital is nearly pure 4d in Ag_2, and the $2\sigma_g$ nearly pure 5s. Figure 7 provides a pictorial representation of the difference between the $2\sigma_g$ wave functions of the two molecules. The unoccupied orbitals are similar in the two; the lowest energy $2\sigma_u$ is essentially s, as seen pictorially in Figure 8, and the higher lying $2\pi_u$ and $3\sigma_g$ are essentially p.

The symmetry of the occupied orbital manifolds alone dictates that there is a net single bond of σ type in both molecules. The relative d-s-p character of this net bonding may be estimated by adding together the percentage contributions of the spherical harmonic in question to the bonding $1\sigma_g$ and $2\sigma_g$ orbitals, and subtracting out the contribution to the antibonding $1\sigma_u$ orbital. The result, using the numbers in Table II, is 73% s, 17% d, and 10% p for Cu_2, compared to 91% s, 1%

Table II. Valence Energy Levels (hartrees) and Charge Distribution for Cu_2 and Ag_2

Cu_2, 2.22 Å							Ag_2, 2.84 Å							Ag_2, 2.47 Å					
$D_{\infty h}$		% charge[a]		Cu sphere[b]			$D_{\infty h}$		% charge[a]		Ag sphere[b]				% charge[a]		Ag sphere[b]		
level	energy	Cu	outer	% d	% s	% p	level	energy	Ag	outer	% d	% s	% p	energy	Ag	outer	% d	% s	% p
$3\sigma_g$	+0.0074[d]	20	81	5	6	89	$3\sigma_g$	−0.0040	20	75	2	2	96	−0.0007	6	93	3	20	77
$2\pi_u$	−0.0309	19	48	7		93	$2\pi_u$	−0.0329	21	38	3		97	−0.0363	16	46	4		96
$2\sigma_u$	−0.0732	46	36	8	74	18	$2\sigma_u$	−0.0843	55	24	2	86	12	−0.0685	40	38	4	79	17
$1\sigma_u$[c]	−0.1611	96	1	95	4	1	$2\sigma_g$[c]	−0.1652	68	6	4	89	7	−0.1684	56	11	5	89	6
$1\pi_g$	−0.1627	98	1	99		1	$1\sigma_u$	−0.2575	98	0	98	1	1	−0.2467	96	0	96	2	1
$2\sigma_g$	−0.1743	69	8	49	49	2	$1\pi_g$	−0.2629	99	0	100		0	−0.2555	97	0	100		0
$1\delta_u$	−0.1755	98	0	100			$1\delta_u$	−0.2712	98	0	100			−0.2729	97	0	100		
$1\delta_g$	−0.1836	96	1	100			$1\delta_g$	−0.2747	98	0	100			−0.2812	96	0	100		
$1\pi_u$	−0.1992	97	0	99		1	$1\pi_u$	−0.2833	98	0	100		0	−0.2991	96	0	100		0
$1\sigma_g$	−0.2380	100	0	63	28	9	$1\sigma_g$	−0.2975	100	0	95	3	2	−0.3245	100	0	93	4	3

[a] Percentage of electrons within the metal and outside the outer spheres. The balance is in the intersphere region. [b] Relative spherical-harmonic contributions to the charge density within the metal spheres. Note that this represents only a minor fraction of the charge for the $2\pi_u$ and $3\sigma_g$ orbitals. [c] The highest occupied levels. [d] Position estimated from transition-state calculations, where it becomes a bound level.

Table III. Calculated and Experimental Electronic Spectra of Cu_2 and Ag_2 ($\times 10^3$ cm^{-1})

		exptl			
transition	calcd[a]	gas[b]	Ar	Kr	Xe
		Cu_2			
$1\pi_g \rightarrow 2\sigma_u$	24.1 (0.02)	20.4	25.0	25.0	25.0
$2\sigma_g \rightarrow 2\sigma_u$	26.5 (0.32)	21.7	27.0	27.0	27.8
$1\pi_g \rightarrow 2\pi_u$	35.2 (0.15)		38.2	37.0	35.1
$2\sigma_g \rightarrow 2\pi_u$	37.2 (1.02)		41.7/42.4	41.5/42.0	40.5/41.0
$1\delta_g \rightarrow 2\pi_u$	39.5 (0.13)		43.1	42.7	41.7
$1\sigma_g \rightarrow 2\sigma_u$	39.8 (0.36)		44.8	44.0	43.1
$1\sigma_u \rightarrow 3\sigma_g$	43.7 (0.03)				
		Ag_2			
$2\sigma_g \rightarrow 2\sigma_u$	22.0 (0.64), 25.7 (0.63)	23.0	24.3/25.8	25.6	25.6
$2\sigma_g \rightarrow 2\pi_u$	33.2 (1.33), 33.6 (1.37)	37.6	37.8/38.3	35.5/37.0	34.5/35.3
$1\pi_g \rightarrow 2\sigma_u$	43.5 (0.03), 45.6 (0.04)	40.2	44.1	45.0	46.1

[a] All spin- and dipole-allowed transitions below 48 and 51 $\times 10^3$ cm^{-1} for Cu_2 and Ag_2, respectively. For Ag_2, the first value is for 2.84 and the second for 2.47 Å. Oscillator strengths are given in parentheses. [b] 0→0 transitions, from ref 6e for Cu_2 and ref 6f for Ag_2. The weak B←X and D←X bands of Ag_2 at 35.8 and 39.0 $\times 10^3$ cm^{-1}, believed due to forbidden transitions, are omitted.

d, and 8% p for Ag_2 at 2.84 Å (the results at 2.47 Å are the same within 1%). These numbers probably overestimate the d contribution, since they refer only to the charge within the atomic spheres, and the d orbitals are more localized there than the s or p. But coupling them with Figure 7 and other contour maps, we believe a reasonable qualitative conclusion is that the bond in Ag_2 is nearly pure s, while in Cu_2 there is a minor but significant d contribution. This is probably the major factor accounting for the very much shorter calculated bond distance in Cu_2 than in Ag_2. The s orbitals are considerably larger than the d; hence admixture of d character into the s-type bonding orbital should shorten the equilibrium separation over and above the decrease expected merely from the smaller atomic radius of Cu.

Assignment of Electronic Spectra. Table III shows our assignment of the electronic transitions of Cu_2 and Ag_2 observed in the gas phase at 2000–2300 K and in solid inert-gas matrices at 12 K. The calculated positions specifically represent the singlet (spin-allowed) components and include orbital relaxation between ground and excited states.

For Ag_2 in matrices there are three clear regions of absorption (see Figure 5), the two near 25 and 38 $\times 10^3$ cm^{-1} being significantly more intense than the one near 45 $\times 10^3$ cm^{-1}. These three bands appear to correlate in energy and relative intensity with the A←X, C←X, and E←X absorptions observed in the gas phase,[6] allowing for slight matrix shifts. The calculations indeed predict three fully allowed transitions below 51 $\times 10^3$ cm^{-1}, with positions and oscillator strengths corresponding closely to those observed. There is no qualitative, and only a slight quantitative, difference in the predictions at

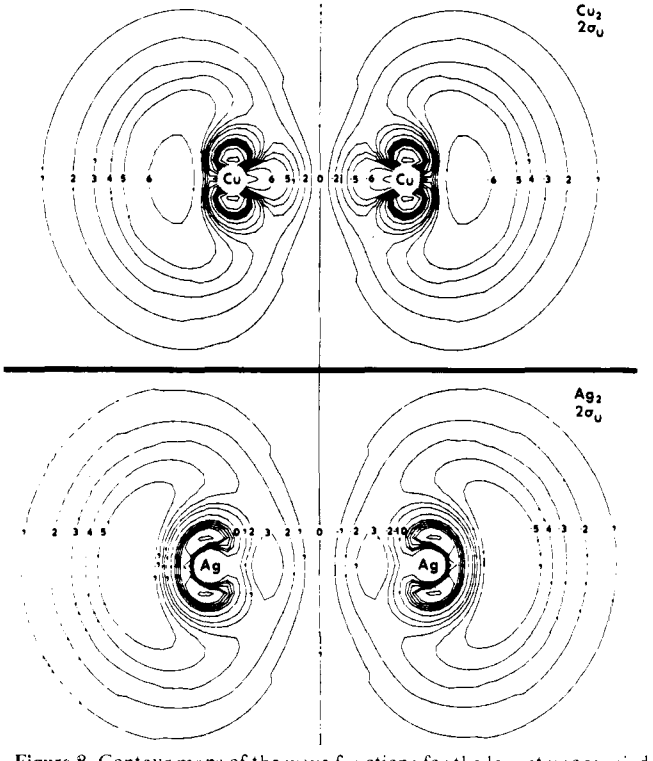

Figure 8. Contour maps of the wave functions for the lowest unoccupied orbitals (mainly s antibonding) of Cu_2 and Ag_2 at 2.22 and 2.84 Å, respectively. The map for Ag_2 at 2.47 Å is similar.

2.84 and 2.47 Å. Moreover, the consensus of careful vibration-rotation analyses of the gas-phase spectrum[6a-c,f] is that the A←X transition is of $^1\Sigma_g^+ \rightarrow {}^1\Sigma_u^+$ type and the C←X of $^1\Sigma_g^+ \rightarrow {}^1\Pi_u$ type, in agreement with our assignments of them as $2\sigma_g \rightarrow 2\sigma_u$ and $2\sigma_g \rightarrow 2\pi_u$, respectively (the character of E←X is uncertain[6f]). Finally, the relative weakness of the E←X transition is in line with our assignment as $1\pi_g \rightarrow 2\sigma_u$, since it is neither especially favored by its $\pi^* \rightarrow \sigma^*$ molecular character (as is A←X by being $\sigma \rightarrow \sigma^*$) nor by its d→s atomic character (as is C←X by being s→p type). The relatively low computed oscillator strength reflects these factors. We have not attempted to assign the weak B←X and D←X bands of Ag_2 observed in the gas phase, but not clearly in the matrix, as we predict several spin- and/or dipole-forbidden transitions which could account for them. It is possible that one of the low-lying shoulders on the second matrix band corresponds to the gas-phase B←X system.

The absorption spectrum of matrix-entrapped Cu_2 (see Figure 3 and Table III) is somewhat less certain than that of Ag_2, owing to band-overlap problems and experimental difficulties encountered in vaporization of the metal in the high metal flux limit. The broad, structured visible feature in the range 340-420 nm is almost certainly due to the matrix-shifted A←X and B←X systems observed for Cu_2 in the gas phase. (It is likely that the high-energy shoulder of the matrix band is due to a secondary trapping site effect and that Cu_2/Cu_3 band overlap is involved in the low-energy shoulder.) The relative intensity of the observed maxima is matrix dependent, while in the gas phase the higher energy B←X system is much more intense.[6a]

There is no gas-phase data available for Cu_2 in the UV region. In the matrix, the range 210-290 nm contains features near 225, 235, and 260 nm which we ascribe to Cu_2, along with weak absorptions probably due to higher Cu_n clusters; the middle band shows two or three distinct maxima. Our assignment of the band near 260 nm to Cu_2 contrasts with that of Moskovits and Hulse,[7b] who believe it due to Cu_3. It has been our experience that the four features near 225, 235, 260, and 370 nm maintain approximately the same relative intensity relationships for different concentration depositions, during photoaggregation and annealing, and importantly during photodissociation of Cu_2 resulting from 370-nm excitation (Figures 3 and 4). For this reason we believe that all four bands are due to Cu_2.

The calculations again predict transitions in close correspondence to the coupled gas-phase and matrix observations (see Table III). The A←X and B←X systems are assigned to $d\pi^* \rightarrow s\sigma^*$ and $s\sigma \rightarrow s\sigma^*$ transitions, respectively. This agrees with the conclusion from the vibration-rotation analysis of the gas-phase spectrum that A←X is of $^1\Sigma_g^+ \rightarrow {}^1\Pi_u$ and B←X of $^1\Sigma_g^+ \rightarrow {}^1\Sigma_u^+$ type.[6d] Moreover, the observation that gas-phase B←X is much stronger than A←X[6a] agrees with the predicted symmetries ($\sigma \rightarrow \sigma^*$ compared to $\pi^* \rightarrow \sigma^*$) and oscillator strengths. It is more difficult to assign the UV region with complete precision owing to the large number of predicted and observed transitions. The 260-nm band seems clearly due to the $d\pi^* \rightarrow p\pi$ transition; the calculations thus provide additional support for our belief that this is a Cu_2 absorption. Based on the predicted relative energies, and especially the oscillator strengths, we assign the main intensity in the 235- and 225-nm bands to $s\sigma \rightarrow p\pi$ and $d\sigma \rightarrow s\sigma^*$, respectively. The $d\delta \rightarrow p\pi$ transition, predicted to be much weaker, may be the high-energy maximum on the 235-nm band.

A unifying feature of these assignments with the photochemical experiments is the fact that the wavelengths used for photoexcitation of both Cu_2 and Ag_2 are essentially those of the $2\sigma_g \rightarrow 2\sigma_u$, i.e., $s\sigma \rightarrow s\sigma^*$, excitation.

Comparison with Other Calculations. Cu_2 and Ag_2 were calculated some years ago by extended Hückel and CNDO methods.[9a,b] It is difficult to compare the results with our own, either because parameters were chosen to fit experiment, poor agreement was obtained when this was not done, or the electronic spectrum was not assigned. An ab initio Hartree-Fock study of the potential curve of Cu_2 has appeared;[26a] the final calculated parameters show comparable or even closer agreement with experiment than our own, but (1) time-consuming configuration-interaction calculations were required to achieve them and (2) the agreement with the experimental r_e is not very meaningful since orbital exponents were adjusted to minimize the total energy of Cu_2 at this distance only. The excited states were not treated in a manner which would allow discussion of the electronic spectrum. Similar comments apply to a very recent ab initio pseudopotential study of Cu_2.[26b] These calculations are of additional interest in that, like ours, they conclude that the 3d electrons play some role in the Cu-Cu bonding. However, since no information about the individual MOs was supplied, it is difficult to precisely compare their conclusions in this area with ours.

Quite recently Anderson has presented a calculation on Cu_2 in which the spectrum was treated, using an extended Hückel method modified to include two-body repulsion terms in the total energy expression.[9c] Parameters were apparently adjusted to match the experimental dissociation energy.[27] The main differences between our energy-level diagram and his at Cu-Cu = 2.22 Å are (1) his d-band width ($1\sigma_g$ to $1\sigma_u$) is about 40% of ours, and (2) his s band is about 6100 cm^{-1} higher relative to the d band than ours, so that the two no longer overlap. With respect to the spectrum, Anderson inverts our prediction that $1\pi_g \rightarrow 2\sigma_u$ is lower than $2\sigma_g \rightarrow 2\sigma_u$, and assigns both the A←X and B←X bands of Cu_2 to components of the $1\pi_g \rightarrow 2\sigma_u$ transition. We prefer our assignment since (1) the experimental vibration-rotation analysis clearly indicates that two transitions are present and that the upper one is $^1\Sigma_g^+ \rightarrow {}^1\Sigma_u^+$,[6d] (2) our photochemical studies and comparison of the spectra of Cu_2 with larger Cu clusters[7b] support our predicted location of $2\sigma_g \rightarrow 2\sigma_u$. Anderson's assignment of the higher energy transitions roughly parallels our own, with two exceptions: (1) he inverts our order of $1\pi_g \rightarrow 2\pi_u$ below $2\sigma_g \rightarrow 2\pi_u$, and (2) he finds $1\sigma_g \rightarrow 2\sigma_u$ much lower (29.0×10^3 cm^{-1}), due to the narrowness of his d band.

Acknowledgments. G.A.O., H.H., D.M., and S.M. gratefully acknowledge financial assistance of the National Research Council of Canada's Operating, New Ideas, and Strategic Energy Grant Programs, the Atkinson Foundation, the Connaught Foundation, Imperial Oil of Canada, Erindale College, and the Lash Miller Chemical Laboratory. D.M. and S.M. express their appreciation to the NRCC for graduate scholarships. J.G.N. and L.N. thank the U.S. National Science Foundation and the donors of the Petroleum Research Fund, administered by the American Chemical Society, for support.

References and Notes

(1) H. Huber and G. A. Ozin, *Inorg. Chem.*, **17**, 155 (1978); G. A. Ozin, *Catal. Rev. Sci. Eng.*, **16**, 191 (1977).
(2) W. Klotzbücher and G. A. Ozin, *J. Am. Chem. Soc.*, **100**, 2262 (1978).
(3) W. Klotzbücher and G. A. Ozin, *Inorg. Chem.*, in press.
(4) (a) D. M. Kolb and D. Leutleff, *Chem. Phys. Lett.*, **55**, 264 (1978; (b) F. Forstmann, D. M. Kolb, D. Leutloff, and W. Schulze, *J. Chem. Phys.*, **66**, 2806 (1977); (c) G. A. Ozin, G. Kenney-Wallace, T. Huber, J. Farrell, and S. Mitchell, paper first presented at the Materials Science Symposium "Small Metal Clusters," Boston, Mass. Nov 1978; to be published; (d) A. A. Belyaeva, Y. B. Predtechenskii, and L. D. Shcherba, *Opt. Spectrosc.*, **34**, 21 (1973).
(5) G. A. Ozin and H. Huber, "Naked Cluster Cryophotochemistry", paper first presented at the ACS symposium "Recent Advances in Metal Cluster Chemistry", Anaheim, Calif., March 1978; *Inorg. Chem.*, in press.
(6) (a) B. Klemen and S. Lindkvist, *Ark. Fys.*, **8**, 333 (1954); **9**, 385 (1955); (b) J. Ruamps, *Ann. Phys. (Paris)*, **4**, 1111 (1959); (c) R. C. Maheshwari, *Indian J. Phys.*, **31**, 368 (1963); (d) N. Åslund, R. F. Barrow, W. G. Richards, and D. N. Travis, *Ark. Fys.*, **30**, 171 (1965); (e) B. Rosen, "Spectroscopic Data Relative to Diatomic Molecules", Pergamon Press, Elmsford, N.Y., 1970; (f) C. M. Brown and M. L. Ginter, *J. Mol. Spectrosc.*, **69**, 25 (1978).

(7) (a) G. A. Ozin and H. Huber, *Inorg. Chem.*, **17**, 155 (1978); (b) M. Moskovits and J. E. Hulse, *J. Chem Phys.*, **67**, 4271 (1977).
(8) K. A. Gingerich, *J. Cryst. Growth*, **9**, 31 (1971).
(9) (a) C. R. Hare, T. P. Sleight, W. Cooper, and G. A. Clarke, *Inorg. Chem.*, **7**, 669 (1968); (b) R. C. Baetzold, *J. Chem. Phys.*, **55**, 4355 (1971); (c) A. B. Anderson, *ibid.*, **68**, 1744 (1978).
(10) (a) W. Klotzbucher, G. A. Ozin, J. G. Norman, Jr., and H. J. Kolari, *Inorg. Chem.*, **16**, 2871 (1977); (b) J. G. Norman, Jr., and H. J. Kolari, *J. Am. Chem. Soc.*, **100**, 791 (1978).
(11) E. P. Kundig, M. Moskovits, and G. A. Ozin, *J. Mol. Struct.*, **14**, 137 (1972).
(12) M. Moskovits and G. A. Ozin, *Appl. Spectrosc.*, **26**, 487 (1972).
(13) K. Schwarz, *Phys. Rev. B*, **5**, 2466 (1972); *Theor. Chim. Acta*, **34**, 225 (1974).
(14) J. G. Norman, Jr., *J. Chem. Phys.*, **61**, 4630 (1974); *Mol. Phys.*, **31**, 1191 (1976).
(15) J. B. Mann, Los Alamos Scientific Laboratory Report No. LA-3690, 1967.
(16) (a) L. Noodleman, *J. Chem. Phys.*, **64**, 2343 (1976); (b) P. S. Bagus and B. I. Bennett, *Int. J. Quantum Chem.*, **9**, 143 (1975); (c) T. Ziegler, A. Rauk, and E. J. Bahrends, *Theor. Chim. Acta*, **43**, 261 (1977).
(17) S. Mitchell and G. A. Ozin, *J. Am. Chem. Soc.*, **100**, 6776 (1978).
(18) For recent reviews see (a) K. H. Johnson, *Annu. Rev. Phys. Chem.*, **26**, 39 (1975); (b) R. P. Messmer in "Modern Theoretical Chemistry", Vol. 8, G. A. Segal, Ed., Plenum Press, New York, 1977, p 215; (c) N. Rösch in "Electrons in Finite and Infinite Structures", P. Phariseau, Ed., Plenum Press, New York, 1977.
(19) For ESR spectra and other properties of the charge distribution, see D. A. Case and M. Karplus, *J. Am. Chem. Soc.*, **99**, 6182 (1977); *Chem. Phys. Lett.*, **39**, 33 (1976).
(20) For deformation densities see R. Salahub, A. E. Foti, and V. H. Smith, Jr., *J. Am. Chem. Soc.*, **99**, 8067 (1977).
(21) Recent examples of interpretation of spectra, structure, and reactivity from our own work include (a) ref 10 and 14; (b) J. G. Norman, Jr., H. J. Kolari, H. B. Gray, and W. C. Trogler, *Inorg. Chem.*, **16**, 987 (1977); (c) J. G. Norman, Jr., *ibid.*, **16**, 1328 (1977); (d) J. G. Norman, Jr., and D. J. Gmur, *J. Am. Chem. Soc.*, **99**, 1446 (1977).
(22) D. R. Salahub, R. P. Messmer, and K. H. Johnson, *Mol. Phys.*, **31**, 529 (1976).
(23) M. Boring and J. W. Moskowitz, *Chem. Phys. Lett.*, **38**, 185 (1976).
(24) J. B. Danese, *J. Chem. Phys.*, **61**, 3071 (1974); *Chem. Phys. Lett.*, **45**, 150 (1977).
(25) L. L. Ames and R. F. Barrow, *Trans. Faraday Soc.*, **63**, 39 (1967).
(26) (a) P. Joyes and M. Leleyter, *J. Phys. B*, **6**, 150 (1973); (b) R. N. Dixon and I. L. Robertson, *Mol. Phys.*, **36**, 1099 (1978).
(27) A. B. Anderson, *J. Chem. Phys.*, **64**, 4046 (1976).
(28) The emission bands not accounted for in this way are thought to originate from concurrent molecular Ag_2^* radiative decay processes, the details of which will be reported in a future publication.
(29) S. Mitchell, D. F. McIntosh, and G. A. Ozin, in preparation.

Macrocyclic Ligand Complexation Kinetics. Solvent, Ring Size, and Macrocyclic Effects on the Formation and Dissociation Reactions of Copper(II)–Cyclic Polythiaether Complexes

Leonard L. Diaddario,[1a] L. Lawrence Zimmer,[1a] Thomas E. Jones,[1a] Lucia S. W. L. Sokol,[1a] Renato B. Cruz,[1a] Edmund L. Yee,[1a] L. A. Ochrymowycz,[1b] and D. B. Rorabacher*[1a]

Contribution from the Department of Chemistry, Wayne State University, Detroit, Michigan 48202, and the Department of Chemistry, University of Wisconsin at Eau Claire, Eau Claire, Wisconsin 54701. *Received July 26, 1977*

Abstract: The kinetics of solvated Cu(II) reacting with a series of open-chain and macrocyclic polythiaethers have been studied in methanol–water mixtures at 25 °C using the stopped-flow and temperature-jump methods. From a determination of the dependence of the formation rate constant values on the solvent composition, it has been established that $Cu(H_2O)_6^{2+}$ represents the only reactive species of solvated Cu(II) over the range of 0–60% CH_3OH (by weight). Based on this observation, aqueous formation and dissociation rate constants have been generated for two open-chain tetrathiaethers, five cyclic tetrathiaethers, and one cyclic pentathiaether (i.e., Me_2- and Et_2-2,3,2-S_4; 12-, 13-, 14-, 15-, and 16-ane-S_4, and 15-ane-S_5). The 25 °C aqueous formation rate constants range from a low of 6.5×10^3 s^{-1} for the smallest macrocycle, 12-ane-S_4, to a high of 4.2×10^6 M^{-1} s^{-1} for the least sterically hindered open-chain ligand, Me_2-2,3,2-S_4, while the dissociation rate constant extremes are 2.6 and 4.5×10^4 s^{-1} for these same two ligand systems, respectively. Aqueous activation parameters have been obtainable for only one ligand system, 15-ane-S_4, for which the formation and dissociation values are $\Delta H_f^{\ddagger}$ (25 °C) = 6.1 kcal mol^{-1}, $\Delta S_f^{\ddagger} = -11$ eu, $\Delta H_d^{\ddagger} = 10$ kcal mol^{-1}, $\Delta S_d^{\ddagger} = -13$ eu. It is concluded that second-bond formation is the probable rate-determining step for all of the cyclic polythiaether complexes studied with the variable difficulty in achieving ring closure accounting for observed differences in the formation rate constants. The primary manifestations of the ring-size effect and the macrocyclic effect are associated with the final steps in the complexation process and, thus, tend to parallel the dissociation rate constants.

Introduction

During the last decade, macrocyclic ligands have attracted widespread attention due to two unique properties: (1) their ability to discriminate among closely related metal ions based on the relative fit of the ligand cavity size to the metal ion radius (*ring size effect*);[2-4] (2) the significant enhancement in complex stability constants which is generally exhibited by optimally fitting macrocyclic ligands relative to their open-chain analogues (*macrocyclic effect*).[2,3,5,6] Both the ring size and macrocyclic effects have been extensively examined from a thermodynamic standpoint[2,3,7-10] and the selectivity patterns are attributed to the combined effects of (1) metal ion solvation, (2) ligand solvation, and (3) ligand conformation,[7,11] the latter two effects being closely coupled. The combination of the foregoing properties is also manifested in the marked increase in membrane permeability exhibited toward selected metal ions when complexed by cyclic polyethers and related open-chain analogues.[12-14]

Largely as a result of the biological interest in the mechanism of metal ion transport, Eigen, Grell, Chock, and others have mounted a concerted effort to investigate the kinetics of alkali metal ions with cyclic polyether antibiotics and with related synthetic crown ethers.[11,15-17] Related studies on

0002-7863/79/1501-3511$01.00/0